

Resonant electron injection as an atomic-scale tool for surface studiesK. Bobrov,^{1,*} L. Soukiassian,¹ A. J. Mayne,¹ G. Dujardin,¹ and A. Hoffman²¹*Laboratoire de Photophysique Moléculaire, Bâtiment 210, Université Paris-Sud, 91405 Orsay Cedex, France*²*Department of Chemistry and Solid State Institute, Technion Israel Institute of Technology, Haifa 32000, Israel*

(Received 1 May 2002; revised manuscript received 26 August 2002; published 7 November 2002)

Three surfaces—clean C(100)-(2×1) diamond, hydrogenated C(100)-(2×1):H diamond and clean Si(100)-(2×1) silicon—were imaged at the atomic scale using the scanning tunneling microscope (STM) operating in an unconventional resonant electron injection mode. The reflection of electrons, forming a resonance in the tip-simple vacuum gap, would seem to play a crucial role in the STM's ability to visualize surfaces under these conditions. The *first* barrier resonance was found to be critical for this surface visualization in two respects. First, a necessary condition was that the STM topographies had to be recorded at a bias coinciding with the energy of the first barrier resonance. Second, the corrugation of the STM topographies was found to be directly proportional to the fineness of the first barrier resonance. Barrier resonances were found to be very sensitive to the difference in energy from the bottom of conduction band. The influence of the bulk electronic structure of the particular sample on the resonance fineness is discussed.

DOI: 10.1103/PhysRevB.66.195403

PACS number(s): 73.20.At, 79.20.Kz

I. INTRODUCTION

Scanning tunneling microscopy (STM) has proven to be a powerful and unique tool for determination of the structural and electronic properties of surfaces.^{1,2} The tip trajectory reveals a STM topography, which represents a convolution of surface topography and local surface density of states.^{1,2} Atomic resolution is achieved due to the *local* nature of the tunneling phenomenon and the extreme sensitivity of tunneling current to the tip-sample separation.^{1,2}

In a recently published paper,³ we have shown that it is possible to obtain atomically resolved images of the insulating diamond surface by the resonance injection of electrons into the conduction band of diamond. In this mode the electrons have a positive kinetic energy after tunneling through a long barrier into the vacuum gap before interacting with the surface. It is common to observe no atomic resolution⁴ in this regime because the field emission current is mainly determined by the electric field in the gap and the tip structure and not by a surface structure. The situation changes *qualitatively* when quantum effects interfere the electron transport. In this case, the long tunnel barrier acts as a filter giving a very localized electron source since only the electrons with a *k*-wave vector perpendicular to the surface arrive in the vacuum. The electron interaction thus depends strongly on the surface electronic structure and so discrete bound electronic states form in the surface potential well in the vacuum created by the surface and the tip.^{5,6} The electron injection manifests itself as barrier resonances or standing waves^{6–8} occurring at biases at which the energy of the emitted electrons matches the energy of the bound states in the potential well.

In this paper we probe the electronic structure of the conduction band by recording barrier resonance spectra, and show that resonant electron injection can be successfully used for visualizing the surface at the atomic scale. The clean diamond, hydrogenated diamond and clean silicon samples have been chosen because they all have the same (2×1) reconstructed surface geometry, consisting of dimer rows:

carbon-carbon dimers in the case of diamond⁹ and Si-Si dimers in the case of silicon.¹⁰ Therefore, here we take advantage of the similar geometry to study the influences of other surface and electronic properties on the barrier resonances. The diamond surfaces (hydrogenated and clean) have been chosen because of the significant effects induced by hydrogen passivation.¹¹

II. EXPERIMENT

Two samples were used in this study: (i) a natural (100) single crystal diamond, 2.5×2.0×0.2 mm³ in size and (ii) a *p*-type silicon (100) sample ($\rho=1\ \Omega\times\text{cm}$), 25×6×0.25 mm³ in size. The diamond sample, prior to insertion into an ultrahigh vacuum chamber, was *ex situ* saturated with hydrogen in a microwave (MW) hydrogen plasma at 800 °C for 1 h. The details on the hydrogenation procedure can be found elsewhere.¹² No special treatment was done to the Si(100) sample, except cleaning in acetone and alcohol to remove organic impurities. Both the diamond and silicon samples were installed into the ultrahigh vacuum (UHV) chamber equipped with the STM (Omicron Vakuumphysik GmbH). Thermal annealing of both samples was done *in situ* in the adjacent UHV chamber ($P<1\times 10^{-10}$ Torr).

The “as-hydrogenated” diamond surface is often contaminated by hydrocarbons, originating from the hydrogenation procedure,¹³ as well as water molecules, which adsorb on the hydrogenated surface from ambient atmosphere.¹⁴ In order to remove these impurities, the diamond surface was *in situ* annealed for 10 min as follows. The diamond was first heated indirectly, by a red-hot tungsten filament located at about 2 cm above the surface. Then, the diamond was heated resistively to about 400 °C ($U=70-90$ VDC, $I=20-60$ mA). Since diamond does not emit light in the infrared region, the diamond temperature was estimated (using an IR pyrometer) from that of the Mo plate holding the sample. The clean diamond surface was obtained by further annealing of the hydrogenated surface *in situ* at 1100 °C (Ref. 12).

The clean silicon surface was prepared by first, outgassing the sample for at least 18 h by resistive heating at 700 °C followed by several flashes at 1050 °C for 20 s each. Between each flash, the sample was slowly cooled down to 700 °C. After several flashes, it was then cooled rapidly to room temperature (RT). The pressure in the UHV chamber during each flash did not exceed 1×10^{-9} mbar.

In this study, the STM was used in two different modes. First, in its conventional tunneling mode² ($U_{\text{bias}} < 4.5$ eV). Second, in an unconventional scanning mode ($U_{\text{bias}} > 4.5$ eV), where the electrons are injected into the conduction band of the surface.³ In both modes, the STM topographies were recorded at constant current. However, the clean diamond surface is insulating so the normal tunnel mode does not work, yet both modes work for the hydrogenated diamond and silicon surfaces since they are conducting.

The surface electronic structure was probed by distance–voltage (Z – V) spectroscopy. The Z – V spectroscopy curves were recorded at positive sample bias simultaneously with the image acquisition. At each chosen location on the surface the tip was positioned and the bias then linearly ramped from +3.5 V up to +10 V. During the bias ramp, the STM feedback retracts the tip from the surface to keep the preset current constant. The corresponding tip displacements as a function of the applied bias, defined as Z – V spectroscopy curves, were then recorded.

III. RESULTS

STM topographies of the clean diamond, hydrogenated diamond and clean silicon surfaces are shown in Figs. 1(a), 1(c), and 1(d), respectively. All were recorded by injecting the electrons into the conduction band of the surface.³ The STM topography of the clean diamond surface, taken at +5.9 V, in Fig. 1(a) shows several domains (labeled as I, II, III, and IV) rotated by 90° and separated by S_A monoatomic steps. A periodic structure ($\Delta \sim 0.5$ nm) of bright and dark lines can be seen within each domain. As proposed in our recent article,³ the interpretation of the images is that the dark lines in Fig. 1(a) represent the dimer rows and bright lines as troughs. This is the only one that is consistent with the structure of the S_A monoatomic step as can be seen by comparing Figs. 1(a) and 1(b). The height profile, recorded perpendicular to the dimer row direction [Fig. 2(a) curve A], gives an average valley-to-peak height variation or topography corrugation of 0.52 Å. For the hydrogenated diamond surface, which is conducting,¹⁴ a flat terrace could be selected using normal tunneling conditions (–1.5 V and 1.0 nA). Then, resonant electron injection at +6.8 V was used to obtain the image shown in Fig. 1(c). Here, the topography corrugation was found to be 0.14 Å from the height profile [curve B, Fig. 2(a)]. This image does not allow an unambiguous assignment of the bright and dark lines as was done for the clean surface [Fig. 1(a)]. So, the thin bright lines plotted in Fig. 1(c) indicate only the direction of the dimer rows. Figure 1(d) represents the STM topography of the clean silicon surface obtained by resonant electron injection at +5.2 V. As in the case of the hydrogenated diamond surface, a flat terrace on the silicon surface was chosen beforehand under

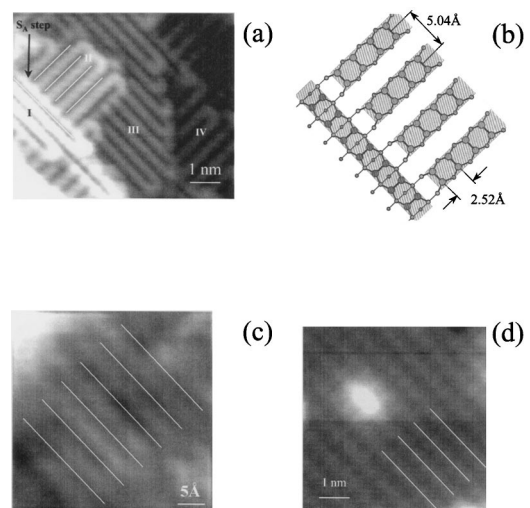


FIG. 1. STM topographies of the diamond and silicon surfaces recorded by resonant injection of the electrons into the conduction band. (a) Clean diamond C(100)-(2×1) surface (6×6 nm, $U_{\text{bias}} = 5.9$ eV, $I_t = 1.0$ nA). The thin white lines indicate the position of the carbon–carbon dimer rows. (b) Top-view on the monoatomic step of the C(100)-(2×1) surface. The top and bottom terraces are marked as I and II, respectively. The filled circles represent the carbon atoms; the largest, the topmost layer and the smaller circles for the subsurface layers. The dimer rows are highlighted by shading whereas the troughs between the dimers are unfilled. (c) Hydrogenated diamond C(100)-(2×1):H surface (3.7×3.7 nm, $U_{\text{bias}} = 6.8$ eV, $I_t = 1.0$ nA). The thin white lines indicate the direction of the carbon–carbon dimer rows. (d) Clean silicon Si(100)-(2×1) surface (6.0×6.0 nm, $U_{\text{bias}} = 5.2$ eV, $I_t = 1.0$ nA). The thin white lines indicate the direction of the silicon–silicon dimer rows.

normal tunnel conditions (–1.5 V, 1.0 nA). For silicon the corrugation is even smaller at 0.04 Å as the height profile shows in curve C of Fig. 2(a). This small corrugation prevents, as in the case of the hydrogenated diamond surface, an unambiguous assignment of the bright and dark lines visible in the STM image.

Figure 3(a) represents the Z – V spectroscopy curves recorded on the clean diamond (curve A), hydrogenated diamond (curve B) and clean silicon (curve C) surfaces. It can be seen that as the sample bias is increased, the outward movement of the tip from the surface is not linear but rather has a steplike trajectory, sometimes only visible as “bumps.” The magnitude of the step-rise and its width is quite different from one surface to the next. For each surface, the first step (marked by the arrows) is always the largest. The highest and narrowest step was observed on the clean diamond surface (curve A), and the smallest step for the silicon surface (curve C), while step for the hydrogenated diamond surface (curve B) is somewhere in between. It is easier to make a quantitative analysis by plotting the derivative dZ/dV [Fig. 3(b)]. The steps in Fig. 3(a) are now clearly seen as peaks in Fig. 3(b) and have been labeled in order of ascending energy, $n = 1, 2$, etc. The Z – V curves were an average of many points on the flat terraces in order to reduce the noise. However, the width of the resonances was the same at any recorded point on the surface.

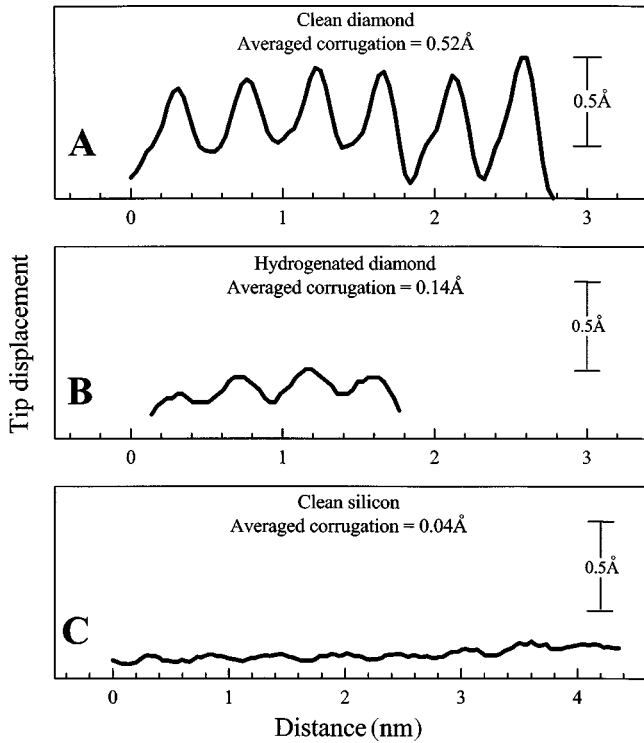


FIG. 2. (a) Height profiles of the clean diamond surface (curve A), hydrogenated diamond surface (curve B), and clean silicon surface (curve C). All the profiles were taken perpendicular to the dimer rows.

IV. DISCUSSION

A. Surface visualization in the resonant electron injection regime

We shall now consider again the Z - V spectroscopy curves shown in Fig. 3(a). At biases lower than the surface vacuum level ($\phi_{\text{Si}}=4.5$ eV, $\phi_{\text{C}}=5.3$ eV) and higher than the bottom of the surface conduction band, electrons normally tunnel through the vacuum gap.^{1,2} For the clean diamond of course this cannot arise since the vacuum level coincides with the bottom of the conduction band and normal tunneling is impossible.³ The situation changes when the bias is higher than that of the surface vacuum level. Now, electrons have positive kinetic energy in the vacuum gap. At certain biases a constructive interference between incident and reflected electrons occurs resulting in a standing wave or barrier resonance. At each resonance, the transmission is highest and so the STM tip retracts more rapidly from the surface revealing the steps in the Z - V curves [Fig. 3(a)], or peaks in the dZ/dV curves. The periodicity clearly demonstrates the oscillatory nature of the interference giving rise to the barrier resonances.

The question that needs to be addressed is what contributes to the observed atomic resolution when injecting electrons into the surfaces? There are two aspects: the barrier resonances and the surface electronic structure. At energies just above the vacuum level of the surface, the electrons coming from the tip have to tunnel through a long barrier before arriving in the vacuum gap above the surface. This barrier acts as a filter allowing through only electrons with a

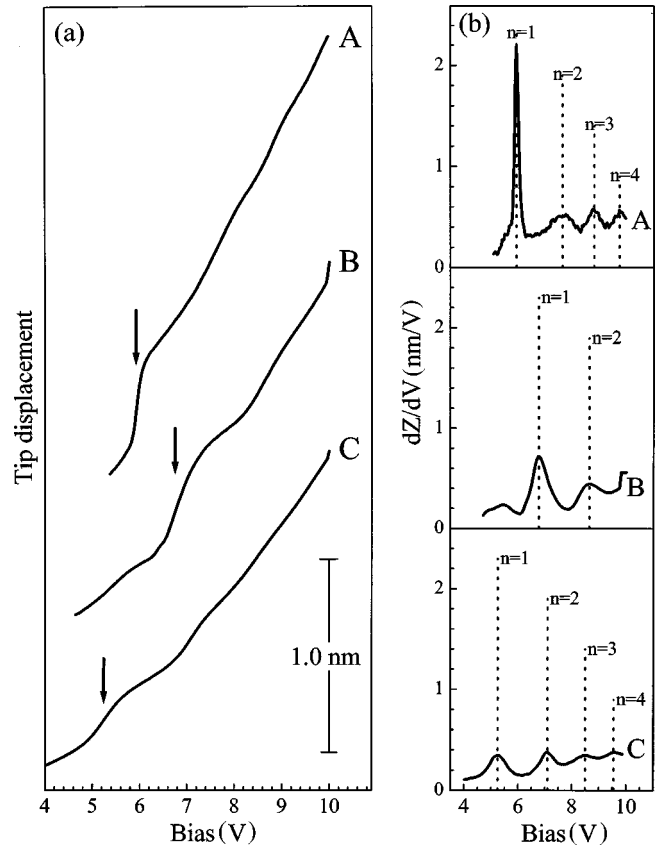


FIG. 3. (a) The distance-voltage (Z - V) spectroscopy curves recorded on the clean diamond surface (curve A), hydrogenated diamond surface (curve B) and clean silicon surface (curve C). For each surface the spectroscopy curves were recorded at the same tunnelling current ($I_t=1.0$ nA) and then averaged over flat terraces. For clarity, these curves are shifted vertically relative to one another. The arrows indicate the position of the first barrier resonance for each surface as deduced from the corresponding dZ/dV curves. (b) The dZ/dV curves obtained by numerical differentiation of the corresponding Z - V spectroscopy curves shown in (a). Curves A, B, and C represent the clean diamond, hydrogenated diamond, and clean silicon surfaces, respectively. The position of the barrier resonances (n) is indicated by the dotted lines.

k -vector perpendicular to the surface. This means that the STM tip, scanning the sample, acts as a very localized source of electrons,¹⁵ both spatially and energetically. The potential well in which the barrier resonances form between the tip and the surface is shown in Fig. 4(a). The potential barrier in the vacuum gap is constructed from a superposition of the electric field induced by the tip, the image potential and the surface potential.^{16,17} Consider now two locations A and B characteristic of the valleys and dimer rows as shown in Fig. 4(c). These locations, A and B correspond to the bright and dark lines seen in the STM topography shown in Fig. 1(a). The observation of dark dimer rows means that the STM tip approaches the surface when passing over the dimer rows. If at location A, for a certain bias and current, resonance conditions between the incident and reflected electrons are satisfied [Fig. 4(b)], then for the same tip-sample separation, at location B, the conditions for resonance will not be satisfied.

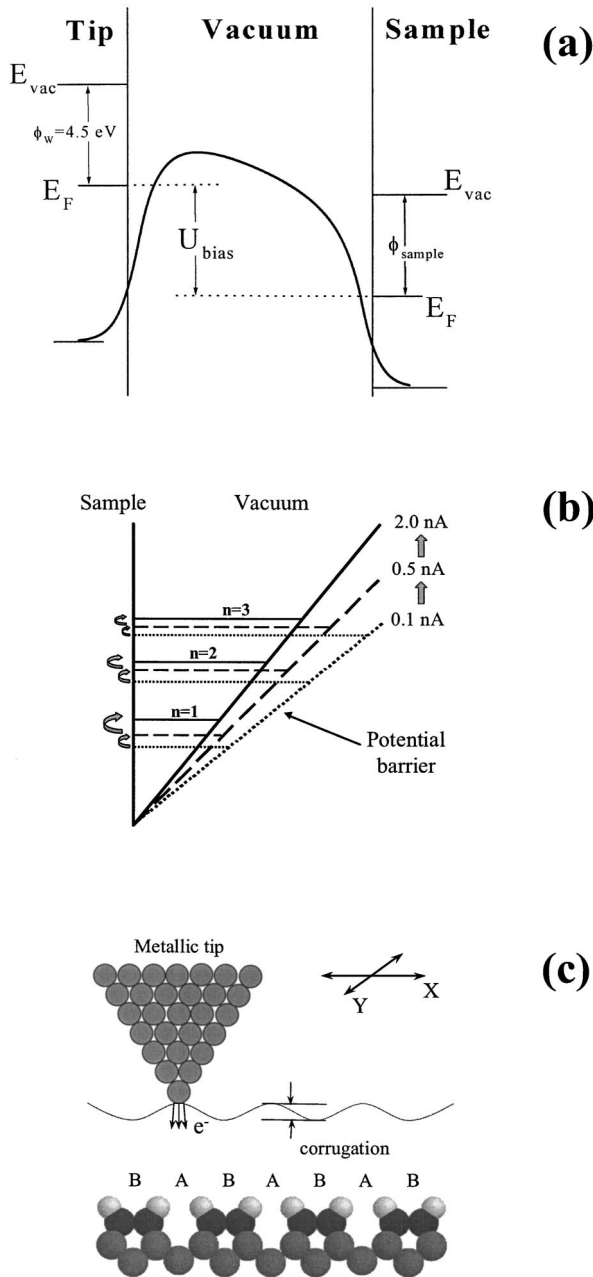


FIG. 4. Surface visualization in the electron injection mode. (a) The potential barrier in the vacuum gap is constructed by a superposition of the electric field and the image potential of the surface, modified to include the surface potential contribution (for more details, see Ref. 16). (b) Schematic of the standing-wave resonance in the surface potential well. For simplicity, the potential well was taken as triangular (Ref. 16). The position of the three barrier resonances ($n=1,2,3$) in the potential well is shown as a function of the preset current. (c) Schematic of the tip scanning the surface. The dotted line represents the tip trajectory when scanning across the dimer rows.

At location B, the same current will be obtained for a smaller tip-sample distance. According to the shape of the $Z(V)$ curve in the vicinity of the first resonance, the resonance energy must be slightly shifted by an amount ΔE towards higher energies at location B compared to location A. The

measured ΔZ corrugation in constant current mode is given by $\Delta Z = (dZ/dV)\Delta E$, where dZ/dV is the slope of the $Z(V)$ curve at the resonance. It follows that the ΔZ corrugation depends both the fineness (dZ/dV) of the resonance and the ΔE corrugation of the resonance energy across the surface. The observation of an atomic-scale ΔZ corrugation requires a similar atomic-scale ΔE corrugation. As schematically shown in Fig. 4, the resonance energy depends on the shape of the potential energy well and at short distances the surface potential. One can therefore explain the ΔE corrugation by atomic-scale variations of the image potential, the surface potential or the phase of the electronic waves reflected from the surface.

This resonant electron injection mode is fundamentally different from that of tunnelling regime. In the tunneling regime, the height variation of the STM tip reflects the local surface density of states, which are laterally corrugated at the atomic scale. However, in the resonant electron injection mode, we probe the atomic scale variation of the interaction between electrons and the surface.

B. The influence of the surface potential well and bulk electronic structure on the surface visualization by resonant electron injection

As we have shown, a necessary condition to visualize surfaces at energies above the surface vacuum level is a resonance arising from incident and reflected electrons in the vacuum gap. In practice STM topographies must be recorded at a bias which corresponds to the energy of the first barrier resonance ($n=1$). Its energy (for a given preset tunneling current) should be determined from the corresponding dZ/dV curves before recording such a STM topography. All the STM topographies, shown in Figs. 1(a), 1(c), and 1(d), have been recorded under such conditions. It was surprising to find that the observable atomic resolution depends on how fine a particular resonance is. The fineness is defined here as the height of the resonance peak in the dZ/dV curves [Fig. 3(b)]. For example, in case of diamond the fineness of the first barrier resonance is given by $dZ/dV = 22 \text{ \AA/V}$. In that case, even small deviation of the bias (more than $\pm 0.1 \text{ eV}$) from the resonance energy induced deterioration of the STM topography and atomic resolution was no longer observed. The first barrier resonance is less fine (7.2 \AA/V) for the hydrogenated diamond surface (curve B). Consequently, a wider bias range ($E_{n=1} = \pm 0.3 \text{ eV}$) could be used to obtain the STM topography shown in Fig. 1(c). In the case of silicon (3.5 \AA/V) the bias corresponded only roughly ($\pm 0.7 \text{ eV}$) to the energy of the first barrier resonance. Furthermore, no STM topographies could be obtained at biases corresponding to the higher lying resonances ($n=2,3$, etc). One of the reasons (amongst others which will be discussed below) seems to be a general loss of sensitivity when the tip retracted from the surface. Indeed, for the second barrier resonance ($n=2$) the tip has to retract by a further 9 \AA for the clean diamond, $\sim 7 \text{ \AA}$ for the hydrogenated diamond and $\sim 4 \text{ \AA}$ for the clean silicon surface as follows from Fig. 3(a).

Despite all the surfaces being visualised at a bias corresponding perfectly to the energy of the first barrier reso-

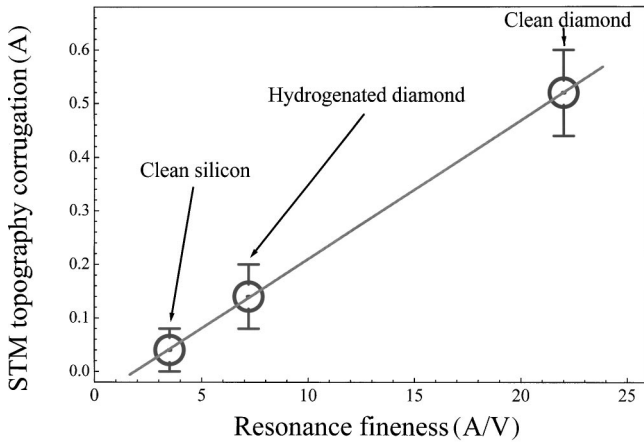


FIG. 5. The corrugation of the STM topographies (Fig. 2) as a function of the first barrier resonance fineness [Fig. 3(b)]. The dotted circles and solid line represent the experimental data and the linear fit, respectively.

nance, the corrugation of the STM topographies are quite different. There seems to be a direct correlation between the fineness of the first barrier resonance and the corrugation of the corresponding STM topography. To confirm this, in Fig. 5 we have plotted the topography corrugation as a function of the resonance fineness. An almost perfect linear dependence is observed: the finer the resonance is, the larger the corrugation is and, consequently, the quality of the STM topography is better. It seems that there is only a slight dependence on the tip apex geometry; barrier resonances recorded using blunt and sharp STM tips have shown essentially the same fineness.¹⁸

The fineness of the particular resonance depends on the reflectivity of the surface,⁷ that is the k -vector change required of the electrons. The magnitude of the change in k -vector is related to, the states potentially accessible whereby the electrons can be elastically scattered and escape along the surface or through the solid. The smaller the available energy window is, the larger is the change in the k -vector. These energy windows are indicated in Fig. 6 as shaded areas in the conduction band, covering the energy range from the conduction band minimum (CBM) to the bias at which the resonance occurs. It is obvious that in this aspect the clean diamond, hydrogenated diamond and clean silicon surfaces are quite different. The wide band gap of diamond¹⁹ of 5.5 eV implies a narrow energy window of only 0.7 eV for the clean diamond surface [Fig. 6(a)]. The energy windows for the hydrogenated diamond and silicon surfaces are 1.9 eV and 4.5 eV, respectively. There is a clear inverse relation with the fineness of the first resonance: 22 Å/V, 7.2 Å/V, and 3.5 Å/V, for the 3 respective surfaces. Now we can easily understand the observed atomic resolution on the clean diamond surface and apparent lack of corrugation on STM topographies for the silicon. Also, for all three surfaces the higher lying resonances have a low fineness, as can be seen in Fig. 3(b) characterized by a large energy window giving rise to a low surface reflectivity. The surface corrugation being so small that no STM topographies could be obtained under such conditions.

Finally it can be seen that very different barrier resonance energies [Fig. 3(b) curves A and B] were obtained for the clean and hydrogenated diamond surfaces. The analysis of the potential barrier in the vacuum gap¹⁶ implies that the

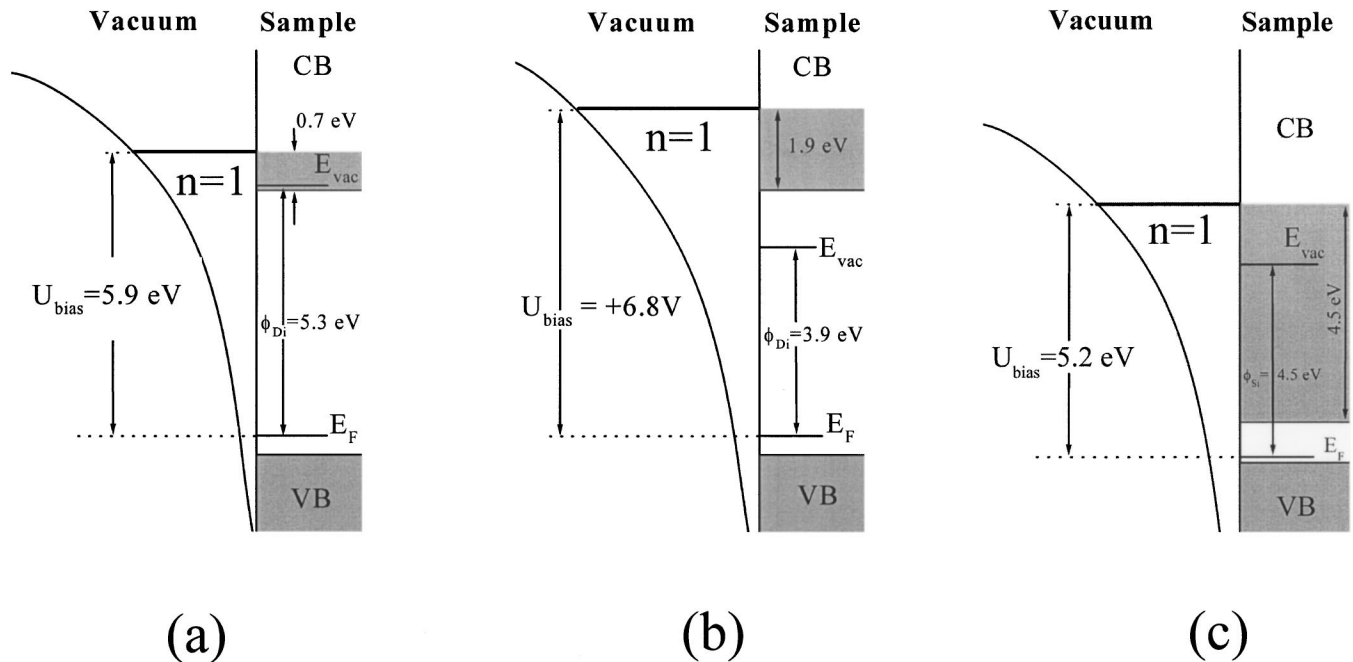


FIG. 6. Schematic of the standing-wave resonance in the surface potential well of (a) the clean diamond, (b) the hydrogenated diamond, and (c) the clean silicon surfaces. For each surface, the position of the first barrier resonance ($n=1$) is marked. VB and CB denote the valence band (always shaded) and conduction band for each surface (at the Γ point). Also the states in the conduction band between the conduction band minimum and the first barrier resonance are highlighted by shading. E_{vac} and E_{F} denote the position of the vacuum level and Fermi level, respectively. For all 3 surfaces, the work functions ($\phi_{\text{Di}}, \phi_{\text{Di}}, \phi_{\text{Si}}$) are shown.

lower work function of the hydrogenated sample ($\phi_{Di} = 3.9$ eV) results in a deeper potential well. The deeper potential well, as we have already discussed in the context the dependence of barrier resonances on the tip-sample separation (Fig. 4), moves all the resonances up in the energy. This model fits our experimental results very well. The first barrier resonance is shifted up by the energy: $E_{n=1} = 5.9$ eV for the clean surface and $E_{n=1} = 6.8$ eV for the hydrogenated one [see Fig. 3(b)]. Also the energy difference (Δ_{1-2}) between the second and the first resonances increases: $\Delta_{1-2} = 1.6$ V for the clean surface and $\Delta_{1-2} = 1.9$ V for the hydrogenated one.

V. CONCLUSIONS

Three surfaces—clean C(100)-(2×1) diamond, hydrogenated C(100)-(2×1):H diamond and clean Si(100)-(2×1) silicon—were visualized by operating the STM in an unconventional resonant electron injection mode. Distance voltage ($Z-V$) spectroscopy reveals the existence of the barrier resonances in the vacuum gap resulting from the interference of incident and reflected electrons on the surfaces. The first barrier resonance was found to be crucial for obtaining atomic resolution for two reasons. First, the coincidence of the bias, at which the STM topographies were recorded, with the en-

ergy of the first barrier resonance was found to be the necessary condition for the surface visualisation. Second, the corrugation of the STM topographies was found to be directly proportional to the fineness of the first barrier resonance. The fineness of the resonances is related to the reflectivity of the surface which depends on the difference of energy between the particular resonance and the conduction band minimum. For conducting surfaces [hydrogenated C(100)-(2×1):H and clean Si(100)-(2×1)] both the usual tunneling and the resonant electron injection modes of the STM can be used. However, for insulating surfaces such as the clean C(100)-(2×1) surface where the usual STM mode cannot be used, resonant electron injection offers a unique method for obtaining atomic-scale STM topographies. The comparison of the 3 surfaces imaged here, confirms the principle of operating the STM in the resonant electron injection mode.

ACKNOWLEDGMENTS

This work is supported by the AFIRST program, the European TMR network “Manipulation of individual atoms and molecules,” and the European IST-FET “Bottom-up-Nanomachines,” (BUN) program.

*Present address: Laboratoire des Collisions Atomiques et Moléculaires, Bâtiment 351, Université Paris-Sud, 91405 Orsay Cedex, France.

¹J. A. Kubby and J. J. Boland, Surf. Sci. Rep. **26**, 61 (1996).

²*Scanning Tunneling Microscopy*, edited by J. Stroscio and W. J. Kaiser (Academic, New York, 1993).

³K. Bobrov, A. J. Mayne, and G. Dujardin, Nature (London) **413**, 616 (2001).

⁴J. J. Sáenz and R. García, Appl. Phys. Lett. **65**, 3022 (1994).

⁵J. A. Kubby and W. J. Greene, Phys. Rev. B **48**, 11249 (1993).

⁶G. Binnig, K. H. Frank, H. Fuchs, N. Garcia, B. Reihl, H. Röhrer, F. Salvan, and A. R. Williams, Phys. Rev. Lett. **55**, 991 (1985).

⁷R. S. Becker, J. A. Golovchenko, and B. S. Swartzentruber, Phys. Rev. Lett. **55**, 987 (1985).

⁸J. A. Kubby, Y. R. Wang, and W. J. Greene, Phys. Rev. B **43**, 9346 (1991).

⁹J. Furthmüller, J. Hafner, and G. Kresse, Phys. Rev. B **53**, 7334 (1996).

¹⁰M. Tsuda, T. Hoshino, S. Oikawa, and I. Ohdomari, Phys. Rev. B

44, 11241 (1991); **44**, 11248 (1991).

¹¹L. Diederich, O. M. Kuttel, P. Aebi, and L. Schlapbach, Surf. Sci. **418**, 219 (1998).

¹²K. Bobrov, H. Shechter, M. Folman, and A. Hoffman, Diamond Relat. Mater. **7**, 170 (1998).

¹³R. Graupner, F. Maier, J. Ristein, L. Ley, and Ch. Jung, Phys. Rev. B **57**, 12397 (1998).

¹⁴F. Maier, M. Riedel, B. Mantel, J. Ristein, and L. Ley, Phys. Rev. Lett. **85**, 3472 (2000).

¹⁵N. Garcia and H. Röhrer, J. Phys.: Condens. Matter **1**, 3737 (1989); N. D. Lang, A. Yacoby, and Y. Imry, Phys. Rev. Lett. **63**, 1499 (1989).

¹⁶J. M. Pitarke, F. Flores, and P. M. Echenique, Surf. Sci. **234**, 1 (1990).

¹⁷G. Borstel and G. Thörner, Surf. Sci. Rep. **8**, 1 (1987).

¹⁸Y. Suganuma and M. Tomitori, Surf. Sci. **438**, 311 (1998).

¹⁹C. D. Clark, P. J. Dean, and P. V. Harris, Proc. R. Soc. London, Ser. A **227**, 312 (1964).